Field Measurements of Rogue Water Waves

MARIOS CHRISTOU*

Shell Global Solutions International B.V., Rijswijk, Netherlands

KEVIN EWANS

Sarawak Shell Berhad, Kuala Lumpur, Malaysia

(Manuscript received 14 September 2013, in final form 17 April 2014)

ABSTRACT

This paper concerns the collation, quality control, and analysis of single-point field measurements from fixed sensors mounted on offshore platforms. In total, the quality-controlled database contains 122 million individual waves, of which 3649 are rogue waves. Geographically, the majority of the field measurements were recorded in the North Sea, with supplementary data from the Gulf of Mexico, the South China Sea, and the North West shelf of Australia. The significant wave height ranged from 0.12 to 15.4 m, the peak period ranged from 1 to 24.7 s, the maximum crest height was 18.5 m, and the maximum recorded wave height was 25.5 m. This paper will describe the offshore installations, instrumentation, and the strict quality control procedure employed to ensure a reliable dataset. An examination of sea state parameters, environmental conditions, and local characteristics is performed to gain an insight into the behavior of rogue waves. Evidence is provided to demonstrate that rogue waves are not governed by sea state parameters. Rather, the results are consistent with rogue waves being merely extraordinary and rare events of the normal population caused by dispersive focusing.

1. Introduction

A rogue water wave is an unexpected large individual wave given the underlying sea state in which it arises. Rogue waves are also referred to as freak or abnormal waves, and they are important for several reasons. One of the key design criteria of an offshore structure is the elevation of the deck. Placing the deck too low will inundate the superstructure and lead to enormous wave-in-deck loads, while a deck that is too high may lead to a prohibitively expensive structure. New offshore structures are designed to avoid wave-in-deck loads by maintaining an effective air gap. In determining the deck elevation, it is necessary to have a good understanding of the short-term variability of the crest height, which will be influenced by the presence of rogue waves. The unexpectedness of a rogue wave can often be more dangerous than the amplitude itself. For example, mariners may interpret an interval of calm as a decreasing sea state (Gemmrich and Garrett 2008), only to be suddenly hit by a large wave event. In addition, maintenance on an offshore platform may be sanctioned in a given sea state without the consideration of an unexpected rogue wave event. Therefore, rogue waves have important health and safety implications.

There have been numerous observations, photographs, and mariners' tales of rogue waves from ocean-going vessels (Nikolkina and Didenkulova 2011). The stories often recount deep holes opening up in the ocean and walls of water (Gibbs and Taylor 2005). These are very useful for postulating theories of the physical mechanism behind rogue waves. However, without actual instrument measurements of the water elevation, any attempts to quantify these effects are difficult to believe. Indeed, for some time the occurrence of rogue waves was thought to be a nautical myth. However, the measurement of the Draupner New Year wave in 1995 provided clear evidence that rogue waves actually exist (Haver and Anderson 2000). It is important to note that the Draupner New Year

* Current affiliation: Department of Civil and Environmental Engineering, Imperial College London, London, United Kingdom.

Corresponding author address: Marios Christou, Department of Civil and Environmental Engineering, Skempton Building, Imperial College Road, South Kensington Campus, Imperial College London, London, SW7 2AZ, United Kingdom.
E-mail: marios.christou@imperial.ac.uk

DOI: 10.1175/JPO-D-13-0199.1

wave was associated with wave loading on the underside of the deck, which provided corroborating evidence of the height of the crest and ruled out the possibility of instrument measuring error.

The Draupner New Year wave has been analyzed in great detail (Walker et al. 2004; Cherneva and Guedes Soares 2008; Adcock et al. 2011; Clauss and Klein 2011). While it was a significant event, one must bear in mind that it is only a single rogue wave and concrete conclusions of a stochastic system such as the ocean cannot be drawn from a sample of one. However, obtaining a large sample of rogue waves is inherently difficult because they are such rare events and field measurements are generally only recorded at single points in the vast ocean. Indeed, Haver and Anderson (2000) have commented that the scarcity of rogue wave measurements makes it difficult to determine whether they conform to standard statistical models.

To address this, it is necessary to accumulate a very large database of field measurements and hope that it will capture some rogue wave events. However, this necessitates storing the raw time history of the water surface elevation. In the past, only the sea state parameters were saved and the raw measurement of the water surface elevation was discarded due to computational storage constraints. Indeed, rogue waves were also often removed from the time trace, as they were considered to be anomalies due to instrument errors. In recent times, with an abundance of cheap computational storage, the time history of the raw wave measurements is also saved. This step change has permitted the detailed analysis of rogue waves, without which the present study could not have been undertaken.

As field measurements are associated with instrument errors, a vast amount of quality control (QC) is required. To produce a reliable database, a strict QC procedure is necessary; however, this has the undesired effect of reducing the amount of data available for analysis. Consequently, the only way to form both a large and reliable database is to collect vast amounts of raw wave data. The importance of a reliable database that can be trusted cannot be stressed enough; no matter how sophisticated the analysis, an unreliable database will lead to wrong conclusions.

The present study describes the formation of such a large and reliable database and its subsequent examination. This paper continues in section 2 with a brief summary of the background on rogue waves and field measurements. For a more detailed review, the reader is directed to Dysthe et al. (2008). Section 3 describes the offshore installations, instrumentation, and quality control procedure for the field measurements. An examination of the influence of sea state parameters, environmental conditions, and local parameters on the formation of rogue waves is then presented in section 4. Conclusions are discussed in section 5.

2. Background

There are several definitions of a rogue wave within the literature; however, all are based on the wave height or crest height being larger than some multiple of the significant wave height. The present study defines a rogue wave within a 20-min sample according to Haver (2000):

$$\frac{\eta_c}{H_s} > 1.25 \quad \text{and/or} \quad \frac{H}{H_s} > 2, \tag{1}$$

where η_c is the crest height (defined as the maximum elevation between zero crossings), H is the wave height, and H_s is the significant wave height, which is the value based on the zeroth spectral moment m_0. Note that either the crest or wave height criteria by themselves are sufficient for the definition of a rogue wave; there is no requirement that both of these criteria are satisfied such as given by Tomita and Kawamura (2000).

A substantial effort has been made to try to explain the occurrence and nature of extraordinarily large wave events. Two almost contradictory mechanisms have been offered for crests substantially higher than predicted by design codes. The first is that the dynamics of unidirectional or very long-crested waves are qualitatively different from directionally spread waves. The fully nonlinear calculations of Gibson and Swan (2007) show that in unidirectional seas the largest waves can be much higher than would be predicted by second-order theory. Several studies based on experimental measurements support this conclusion (Onorato et al. 2006; Fedele 2008; Cherneva et al. 2009, 2013; Latheef and Swan 2013). On the other hand, Donelan and Magnusson (2005) have suggested that crossing seas might lead to exceptionally high crests. Second-order simulations (Toffolli et al. 2006; Christou et al. 2009) do show slightly higher crests in crossing seas. As such, field measurements in a variety of environments must be studied to provide evidence of physical mechanisms creating rogue wave events.

One problem with field measurements is that most routine and operational wave measuring programs employ surface-following buoys. Although these provide reliable estimates of the usual sea state parameters, such as significant wave height and wave periods, they tend to underestimate the crest height of individual waves (Krogstad and Barstow 2000; Casas-Prat and Holthuijsen 2010). Furthermore, in the extreme cases, it is thought that the buoy may be dragged through the crest or skirt around a short-crested wave (Seymour and Castel 1998).

There have been some large databases of field measurements recorded by surface-following buoys. Pinho et al. (2004) measured 1.2×10^6 waves in the Campos basin offshore of Brazil, and Casas-Prat and Holthuijsen (2010) analyzed 10×10^6 individual waves measured off the Catalan coast in Spain.

With 122×10^6 individual waves, the present study has an order of magnitude more data than Casas-Prat and Holthuijsen (2010). Furthermore, the present database was collected from fixed instruments on offshore platforms, which are capable of accurately measuring crest heights. Dysthe et al. (2008) commented that measurements from fixed instruments give the most reliable information on rogue waves. Indeed, this is the reason why only data from fixed instruments have been collected in the present study. As far as the authors are aware, the largest database of raw wave data from fixed instruments was collected by Olagnon and van Iseghem (2000), who measured 1.6×10^6 waves using a Plessey wave radar on the Frigg platform in the North Sea. Therefore, the present database is two orders of magnitude larger. As mentioned in the introduction, a large and reliable database is essential to be confident of the conclusions on rogue wave behavior.

3. Description of field measurements

a. Offshore installations

Raw measurements of the water surface elevation were gratefully provided by the following sponsors of the Cooperative Research on Extreme Seas and Their Impact (CresT) Joint Industry Project: Anardarko, BP, ConocoPhillips, Shell, Statoil, Total, and Woodside. In addition, there were sources of data from the Wave Crest Sensor Intercomparison Study Joint Industry Project (WACSIS JIP) and the public domain. The majority of the data were recorded from fixed jacket structures. However, in a minority of cases the measurements were taken from tension leg platforms (TLPs) or spars, for which the raw wave measurement was adjusted to account for the recorded motion of the floating platforms. In total, there were 22 installations in the North Sea, 5 in the Gulf of Mexico, 5 in the South China Sea, and 1 on the North West shelf of Australia. The source, geographic location, platform name, water depth, and sensor type for the whole dataset are presented in Table 1.

As far as the period of the dataset is concerned, the earliest sample is from August 1969 and the latest is from April 2008; however, this is by no means continuous. Most of the raw wave samples from the North Sea and the South China Sea (which represent the majority of the dataset) are continuous over a span of 3 yr. The datasets from the Gulf of Mexico and the North West shelf of Australia are sporadic, and the data provided were only recorded during large storms and hurricanes (or tropical cyclones). The installations were located in mean water depths ranging from 7.7 to 1311 m.

b. Instrumentation

The majority of the data were recorded on Shell installations using the Saab radar, which accounted for approximately 94% of the measured wave samples in the whole database. For that reason, this section will principally describe the Saab WaveRadar REX and only briefly mention the other sensors employed.

The Saab WaveRadar REX (hereafter referred to as Saab radar) is manufactured by Saab Rosemount, and it was first introduced in 1994 as a derivative of their TankRadar system. It uses a low power (<0.5 mW) frequency, modulated (9.7 to 10.3 GHz, with a linear sweep), continuous microwave signal. The transmitted signal changes frequency during the time taken for the reflected signal to return. The frequency of the received signal reflected from the surface is compared to the transmitted signal frequency, and the difference in frequency is proportional to the distance to the surface of the water. Digital filtering and FFT calculations are used to counter disturbances and maintain measurement accuracy. During the recording cycle of 10 Hz, a number of measurements are produced and an average distance recorded. The manufacturer specifications quote an accuracy that depends on the range, which is between 3 and 65 m from the TRL/2 adaptor (the measurement datum). For a range less than 50 m, the accuracy is ± 6 mm, whereas for a range greater than 50 m, the accuracy is ± 12 mm. The beamwidth has a 10° included angle. For the installations in the present study that employed the Saab radar, the distance from the instrument to the mean water level ranged between 14.2 (South China Sea) and 34.3 m (North Sea); consequently, the accuracy is ± 6 mm. In addition, because of the antenna beam pattern and subsequent signal processing, the target footprint on the ocean surface is generally constrained to $\pm 2°$. The manufacturer claims that every Saab radar is calibrated by Rosemount in a special calibration facility. Because of the design and construction of the electronic and microwave unit, the Saab radar calibration is extremely stable and periodic recalibration is not required. The Marex radar and Endress+Hauser FMR130 radar were also employed as instrumentation on some of the offshore installations. These are both based on similar principals as the Saab radar.

With 6.2% of the total waves recorded in the database, the laser sensors were the second most abundant

TABLE 1. Source, geographic location, mean water depth, and sensor for each installation within the database.

Source	Location	Platform	Depth (m)	Sensor
Anardarko	Gulf of Mexico	Marco Polo	1311	EH radar[a]
BP	Gulf of Mexico	Holstein	1308	Saab radar
		Marlin	988	Saab radar
ConocoPhillips	North Sea	Ekofisk	75	Optech laser
Public Domain	Gulf of Mexico	Open sea	100	Wave staff
Shell	North Sea	Auk	85	Saab radar
		AWG	7	Saab radar
		Brent	141	Saab radar
		Clipper	21	Saab radar
		Cormorant	149	Saab radar
		Dunlin	152	Saab radar
		F03	42	Saab radar
		Gannet	95	Saab radar
		Goldeneye	122	Saab radar
		K14	27	Saab radar
		L09	25	Saab radar
		Leman	36	Saab radar
		Nelson	85	Saab radar
		North Cormorant	161	Saab radar
		Sean	32	Saab radar
		Shearwater	90	Saab radar
		Tern	170	Marex radar
				EMI laser
	South China Sea	E11	70	Saab radar
		F6	87	Saab radar
		KN	54	Saab radar
		M3	115	Saab radar
		SF	49	Saab radar
Statoil	North Sea	Draupner	70	Laser
		Kvitebjørn	190	Saab radar
Total	North Sea	North Alwyn	126	EMI laser
	Gulf of Mexico	Matterhorn	869	EH radar[a]
WACSIS JIP	North Sea	Noordwijk	18	EMI laser
				Marex radar
				Saab radar
				Wave staff[b]
				Step gauge[c]
Woodside	Northwest Australia	North Rankine A	125 m	Saab radar

[a] Endress+Hauser FMR130 radar.
[b] Baylor wave staff.
[c] Vlissingenbaak step gauge.

type of instrument used for the present field measurements. The EMI laser is a pulsed range finder operating in the near-infrared region. Narrow pulses of light are produced by a laser diode, and the radiation from the target is used to stop a time interval measurement. The time of travel is converted to an analog voltage proportional to the distance to the reflector. The response of the optical unit is 10 to 15 Hz, but the output is usually filtered by a 2-Hz Butterworth filter to eliminate high-frequency noise. Angevaare (1986) specifies that the instrument can measure to within an accuracy of 0.1 m for wave heights between 0 and 10 m and to within 1% for wave heights between 10 and 50 m. The transmitter has a maximum beamwidth of 1°, and therefore the EMI laser has a much narrower footprint than the radars. However, Crabb et al. (1983) report measurements made from a platform in Christchurch Bay with an EMI laser, during which the sensor was affected by fog, occasionally demonstrating a low-amplitude noise-dominated signal due to fog (backscatter), but independent of wave height. The other laser employed was the Optech laser, which is a pulsed infrared laser and can measure wave height in the range of 0.3 to 50 m with an absolute accuracy of 2 cm and operational accuracy of 5 cm.

A typical instrument for wave measurements from platforms in the Gulf of Mexico is the Baylor wave staff, which consists of a pair of stainless steel wire ropes separated by insulators about 20 cm long. The transducer

measures the natural frequency of the inductive loop made by the two wires and the sea surface, from which the length of the loop is found. The instrument is robust and relatively immune to fouling.

Finally, the Vlissingenbaak step gauge is a wave and tide measuring system produced by Etrometa Holland and is based on the measurement of conductivity to seawater of equally spaced electrodes. It consists of a 15-m-long metal pole with electrodes isolated from the pole and connected via a cable connector combination to the electronic unit where the highest wet electrode is detected and where a check is performed on defective electrodes. Measurements are performed at 10 Hz.

An important consideration for the instrumentation is their location on the platform, such that they measure only the undisturbed wave field (Forristall 2005). As such, the instruments were placed as far away as feasibly possible from the platform legs and upwave of the dominant mean wave directions.

c. *Quality control of raw wave data*

Field measurements are associated with instrument errors such as lock-ins, dropouts, and spikes. To produce a reliable database that can be trusted, a strict QC procedure is necessary to identify and remove these errors. As mentioned above, the quality of the database is essential, and no matter how sophisticated the analysis performed, poor data will lead to incorrect conclusions. The first step of any automatic QC procedure for raw wave data consists of defining a series of error flags. The number of occurrences of these error flags within a wave sample then determines whether the sample passes or fails the QC check. The field measurements were first divided into 20-min wave samples in order to ensure stationarity. Then for each sample, the error flags described below were employed:

Flag 1: Number of occurrences of 10 consecutive points of equal value.
Flag 2: Number of zero upcrossing wave periods longer than 25 s.
Flag 3: Number of occurrences that the limit rate of change is exceeded. The limit rate of change of the water surface elevation S_y is given by $S_y = (2\pi\sigma/T_z)\sqrt{2\ln N_z}$, where σ is the standard deviation, N_z is the number of zero upcrossing periods, $T_z = N/(s_r N_z)$ is the mean zero upcrossing period, with N being the number of points in the time history of the surface elevation and s_r being the sample rate.
Flag 4: Number of consecutive errors of flag 3.
Flag 5: Number of crest elevations greater than 5 times the standard deviation of the water surface elevation.
Flag 6: Number of consecutive errors of flag 5.
Flag 7: The amount of energy in the spectrum below 0.04 Hz is greater than 5%.
Flag 8: The amount of energy in the spectrum above 0.60 Hz is greater than 5%.

During operations at offshore installations, the principle quantities of interest are the sea state parameters and the maximum wave and crest heights. Consequently, all the error flags above can occur a predefined number of times before a raw wave sample is rejected. However, as the present study is performing a detailed analysis of the raw wave data, it was decided to use a very strict automatic QC procedure. This involved rejecting raw data that contained any error flags, and consequently the wave samples that passed did not contain any of the errors described above. This ensured a high-quality dataset that is very reliable, which can be interrogated to test any particular hypothesis, and the results can be interpreted with a high level of confidence that the underlying data are error free. In doing so, it was found that flag 3 was too strict, and therefore the double temporal derivative of the water surface elevation was also checked against S_y, and only when both were larger than the limit did the sample fail.

With the error flags defined and the very strict method employed, the key steps of the QC procedure are as summarized below:

(i) Divide the raw wave data into 20-min samples, demean the time trace, and calculate the parameters (H, η_c, H_s, T_p, ...) using the zero upcrossings method.
(ii) Determine whether or not the sample contains a rogue wave according to the definition of Haver (2000).
(iii) There are now two paths that can be followed:
    1) Normal wave sample—If there are no rogue waves in the sample, apply the very strict automatic QC method described above. If the sample passes, then further analysis can be performed; a failed sample is discarded.
    2) Rogue wave sample—If there is a rogue wave in the sample, first apply the very strict automatic QC method, but without imposing flag 5, as this would automatically fail due to the large crest elevations. If the sample passes, then it moves on to a visual QC check; a failed sample at this stage is discarded. The visual QC check consists of looking at the water surface elevation of the rogue wave and deciding if it looks plausible. If the sample passes, further analysis can be performed; a failed sample is discarded.

Clearly, the visual QC check performed on the rogue waves is a highly subjective criterion, but there was no automatic procedure that could be applied with confidence. Furthermore, one could argue that the shape of rogue waves is not known for certain. However, during the process of looking through vast quantities of raw wave data from numerous installations around the world, the authors accumulated good experience of detecting the typical errors of the various wave sensors. This was especially useful in performing the visual QC checks of the rogue waves. The quality control procedure has been both extensive and exhaustive.

Overall, 82% of the normal wave samples passed the QC checks, leading to 528 475 20-min sea states. Whereas only 16% of the rogue wave samples passed, leading to 3649 20-min sea states. This created a reliable database of 122 million individual waves. Within the quality-controlled database, the significant wave height covered the range $0.12\,\text{m} \leq H_s \leq 15.4\,\text{m}$, the peak period was $1\,\text{s} \leq T_p \leq 24.7\,\text{s}$, the maximum crest height was 18.5 m, and the maximum recorded wave height was 25.5 m. The majority of the raw wave data were measured in the North Sea (81% of normal waves and 92% of rogue waves).

The ratio of rogue waves to total waves is largest in the Gulf of Mexico followed by the North West shelf of Australia. The raw wave data from these two regions were only provided during times when hurricanes (or tropical cyclones) passed close to the offshore installations. In contrast, the North Sea measurements were supplied in the form of continuous datasets. Consequently, there were approximately 100 million waves recorded in the North Sea, whereas the Gulf of Mexico consisted of only 85 400 waves. The difference of three orders of magnitude in sample size may well explain the larger ratio in the Gulf of Mexico compared to the North Sea; clearly the latter dataset is considered to provide a more reliable estimate of the ratio of rogue to normal wave samples. Another possible explanation though is that steeper seas are more likely during hurricanes (or tropical cyclones), which may be more conducive to creating rogue wave events. The works of Latheef and Swan (2013) and Cherneva et al. (2013) have demonstrated that sea state steepness is important, and as such, its effect on rogue wave samples will be examined further in the following section.

As the conditions in the North Sea vary depending on location, it can be further subdivided into its three main regions—northern, central, and southern. In doing this, the northern North Sea only contains 10.9% of the total waves and 19.9% of the rogue wave samples in the whole database. Consequently, the majority of the data were measured in the central and southern North Sea. Therefore, the results that will be discussed in the next section are representative of waves propagating in intermediate water depths within extratropical locations.

4. Discussion of results

a. Sea state parameters

This section will examine whether there is a link between the characteristic sea state parameters and the likelihood of rogue wave events. An interesting parameter to examine first is sea state steepness, which could be an explanation for rogue wave events occurring, especially extreme crests. This is because the design distributions for crest heights are based on second-order theory, whereas it is known that nonlinear wave–wave interactions beyond second order can provide significant increases in the crest elevation, especially in long-crested seas (Gibson and Swan 2007).

The sea state steepness is typically represented by plotting the significant wave height H_s against the peak period T_p, which is shown in Fig. 1a. This figure represents all sea states that passed the QC procedure with a single dot, and the rogue wave samples are distinguished from the normal wave samples. While Fig. 1a shows that the cloud formed by rogue wave sea states are clustered more toward the steep wave part of the plot, they nevertheless fall completely within the large number of normal wave samples. It is also clear from the figure that there are many normal sea states that are steep; thus, wave steepness cannot be the sole cause of these rogue wave events.

Figures 2a and 2b illustrate the maximum crest heights for each 20-min sample as a function of the mean steepness and skewness, respectively. Each of these is a sea state parameter that may indicate a link to the formation of rogue waves, and they will be considered in turn. First, consider the mean steepness S_1 as defined by

$$S_1 = \frac{2\pi}{g}\frac{H_s}{T_1^2}, \tag{2}$$

where g is the gravitational acceleration, and T_1 is the mean wave period calculated from the ratio of the first two moments of the wave spectrum m_0/m_1. This is presented in Fig. 2a and is similar to Fig. 1a, using the mean wave period T_1 instead of the peak wave period T_p to take advantage of the increased stability of T_1. It is clear that Fig. 2a is not materially different from Fig. 1a and does not change our conclusion that sea state steepness plays no governing role in the formation of rogue waves.

Second, Fig. 2b illustrates the influence of the skewness of the sea state. Once again, the skewness of the rogue wave samples falls within the bounds of those for

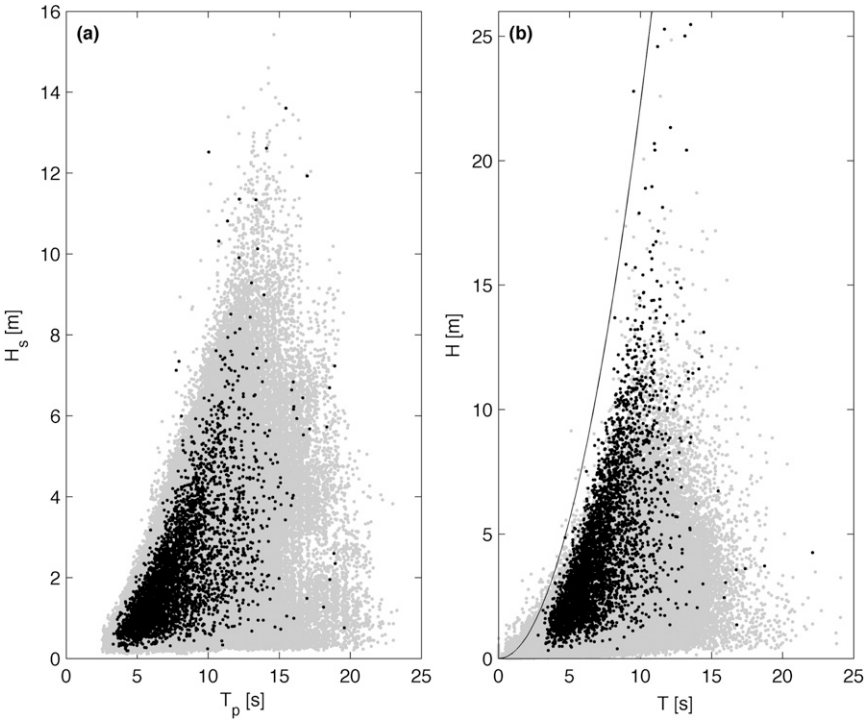

FIG. 1. (a) Significant wave height vs peak period indicating sea state steepness for 20-min normal wave samples (gray dots) and rogue wave samples (black dots). (b) Individual wave height vs period indicating individual wave steepness for normal waves (gray dots) and rogue waves (black dots) and one-seventh steepness curve (black line).

normal sea states. Therefore, there is no indication that the skewness of the sea state alone might indicate the likelihood of the occurrence of a rogue wave.

Figure 3a presents the maximum crest heights for each 20-min sample as a function of the kurtosis of the sea state. In this case, there appears to be a pattern with all the rogue wave samples having a value greater than three. However, this is misleading, as a rogue wave by definition has a water surface elevation significantly larger than the rest of the waves in the sample, and the record will have a high kurtosis value as a consequence. As such, Fig. 3a is merely reiterating the definition of a rogue wave. Evidence for this is provided by Stansell (2004), who analyzed field measurements and also found that sea states containing rogue waves had large kurtosis values. On removing the rogue wave from the sea state and recalculating the kurtosis of the remaining water surface elevation, Stansell (2004) found that the kurtosis returned to normal levels, as expected. This same procedure was performed on the present database and results in Fig. 3b. As the cloud for the kurtosis of the rogue wave samples completely lies within that of the normal wave samples, Fig. 3b confirms the findings of Stansell (2004). Therefore, a high kurtosis simply indicates the presence of a single rogue wave in a sea state, rather than being a measure of the likelihood of observing a rogue event.

In addition, the shapes of the variance density spectra of rogue wave samples were visually examined for the presence of uni- or bimodal conditions. However, there were no observable trends with both unimodal and bimodal frequency spectra occurring. This suggests that rogue waves can form in pure wind seas, pure swells, or a combination of wind seas and swells. Therefore, crossing seas that have been hypothesized as the cause of rogue waves (Adcock et al. 2011) cannot be the sole explanation of these rare events. Once again, it does not appear that the underlying sea state conditions influence the formation of rogue waves.

b. *Environmental conditions*

This section examines whether the rogue waves within the database were created in similar environmental conditions, which would indicate a possible physical mechanism for their formation. This involves examining the wind, wind-sea waves, swell waves, currents, and relative conditions between these environmental conditions during the rogue wave events. It is important to note that the environmental conditions that generate rogue waves cannot be analyzed in isolation from those that

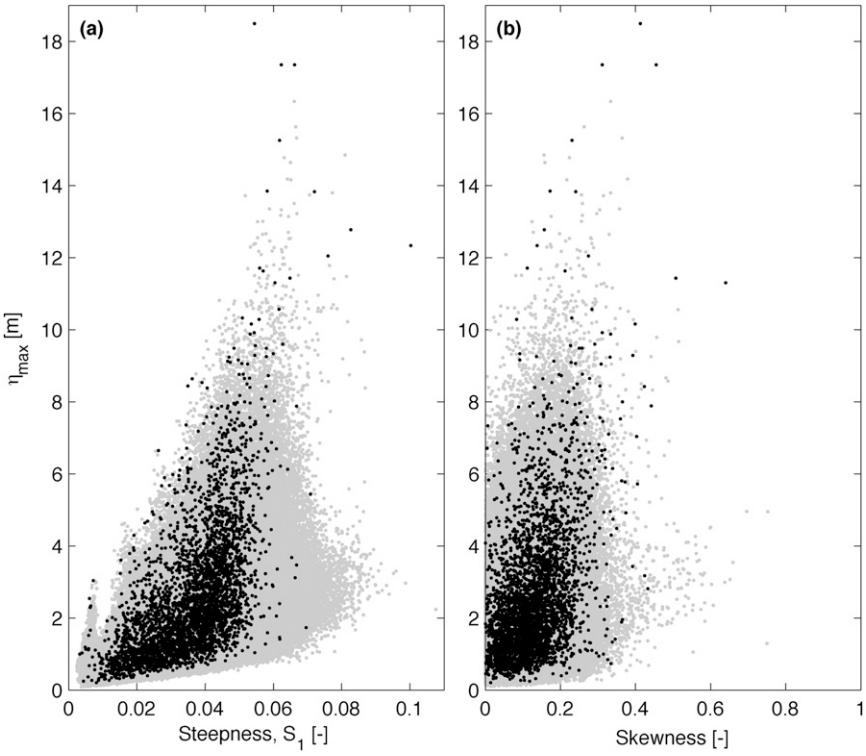

FIG. 2. (a) Maximum crest height vs mean sea state steepness S_1 and (b) skewness of 20-min normal wave samples (gray dots) and rogue wave samples (black dots).

cause normal wave samples. This is because if a certain environmental condition that results in a rogue wave can also lead to a normal wave sample, then it cannot be a factor conducive to forming rogue waves. This would only confirm that there must be an additional mechanism in place for forming the rogue wave. Therefore, the environmental conditions present during normal and rogue wave events were both examined.

As mentioned above, the majority of the rogue waves occurred in the North Sea, and therefore the focus was on this region. For the present study, the waves and winds were obtained from hindcast data by Oceanweather, Inc. (Cardone and Cox 2011). The hindcast simulation was specifically run for the present study over the period of 1 January 2000 to 31 December 2008. The frequency–direction spectra from the hindcast database were then partitioned into wind-sea and swell components using a program called XWaves (Hanson and Phillips 2001). The hindcast grid point that was geographically closest to the offshore installation was chosen. Furthermore, as the hindcast spectra were output in 1-hourly intervals and the rogue wave samples were 20 min in duration, the hindcast spectrum predicted at the closest time to the rogue wave event was employed. In terms of the current, the tidal component was calculated using the POLPRED software (Proctor et al. 2004). The residual current was not calculated, since the currents in the North Sea are dominated by the tides, and the residual should have a negligible influence on the results.

The absolute environmental conditions at the Goldeneye platform (see Table 1) are presented in Fig. 4 and the relative conditions are presented in Fig. 5. These figures illustrate the empirical probability density function (pdf) of the environmental conditions that created normal waves and of those that formed rogue waves. The hindcast dataset produced 77 083 hourly sea states that represented the normal wave samples. In contrast, at the Goldeneye platform there were 743 rogue wave events, which were the most rogue events at an installation in the database and as such are used as an example. Therefore, the normal wave samples outweigh the rogue waves by two orders of magnitude. The vast difference in sample size should be considered when interpreting Figs. 4 and 5. It can be observed that the pdfs for the normal waves are smoothly varying, whereas those for the rogue waves are quite erratic, which is simply due to the difference in sample size. As mentioned in the introduction, this goes back to the issue of having a large enough database to examine the occurrence of rogue waves and ensuring reliable results.

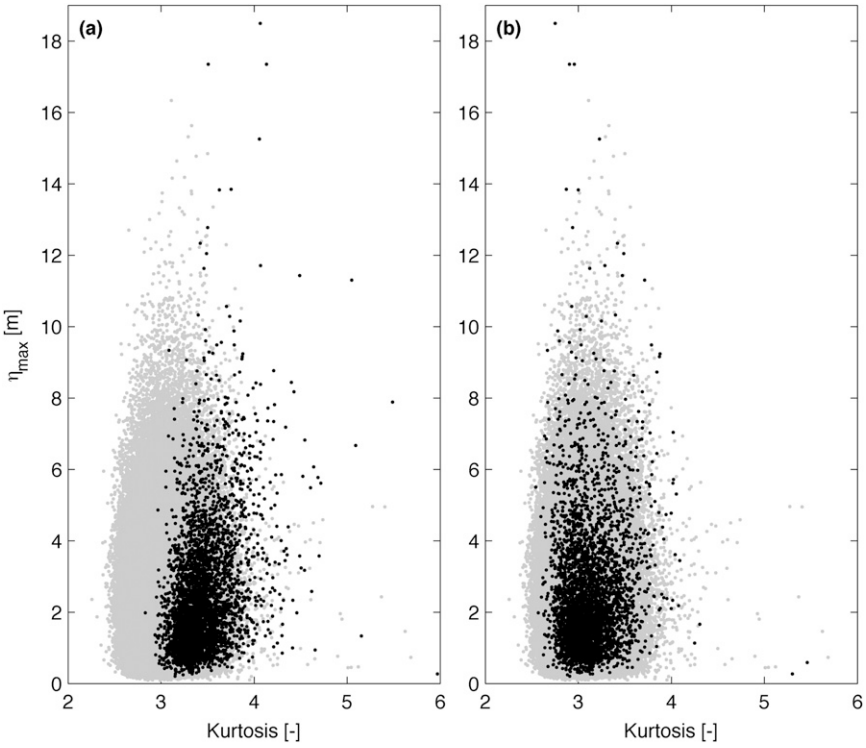

FIG. 3. Maximum crest height vs kurtosis of 20-min wave samples. (a) The normal wave samples (gray dots) and rogue wave samples with the rogue wave event present (black dots). (b) The normal wave samples (gray dots) and rogue wave samples with the individual rogue wave event removed from the 20-min sample (black dots); the kurtosis is then calculated and as such it is not biased by the presence of a rogue wave.

Figures 4a, 4d, 4g, and 4j present the pdfs for the significant wave height H_s, peak period T_p, mean direction of propagation θ_m, and directional spreading σ_s of the wind-sea partition, respectively. Similarly, Figs. 4b, 4e, 4h, and 4k illustrate the pdfs for the same parameters for the swell partition. Figures 4c and 4f show the pdfs of the wind speed and direction, respectively. Likewise, Figs. 4i and 4l present the pdfs of the current speed and direction, respectively.

Figures 5a–c illustrate the pdfs for the relative conditions between wind-sea and swell components for the parameters H_s, T_p, and θ_m, respectively. Finally, Figs. 5d and 5e show the relative direction of propagation between wind sea and current and between swell and current, respectively. It is important to note that out of the 743 rogue wave events at Goldeneye, there were only 189 that contained both wind-sea and swell components; as mentioned in section 4a, uni- and bimodal spectra were both present for rogue wave samples. Therefore, the pdfs of the rogue wave samples for the relative conditions in Fig. 5 are even more erratic than for the absolute environmental conditions. As before, this should be taken into consideration when comparing the pdfs for normal and rogue wave samples.

Examining Figs. 4 and 5, it can be observed that for all parameters the pdfs of the rogue wave samples overlap those for normal waves, especially considering the two orders of magnitude difference in the sample size of the two datasets; there are some differences, but they are generally small. Figure 4c has relatively larger differences and one may be tempted to speculate that higher wind speeds, which affect the wave age and thus steepness of the sea state, could lead to rogue waves. Similarly, one may be tempted to speculate from Fig. 5a that rogue waves formed in bimodal sea states have wind seas with relatively higher H_s when compared to the swell partition. However, both of these observations may also simply be a manifestation of the difference in sample size, but they warrant further investigation in a future study. Aside from this, these figures present evidence to suggest that the environmental conditions that generate normal waves, which are the prevalent conditions in a region, also form rogue waves. Once again, it does not appear that physical processes that operate on a sea state level influence the formation of rogue waves. The next section will examine the influence of local parameters on the appearance of rogue waves.

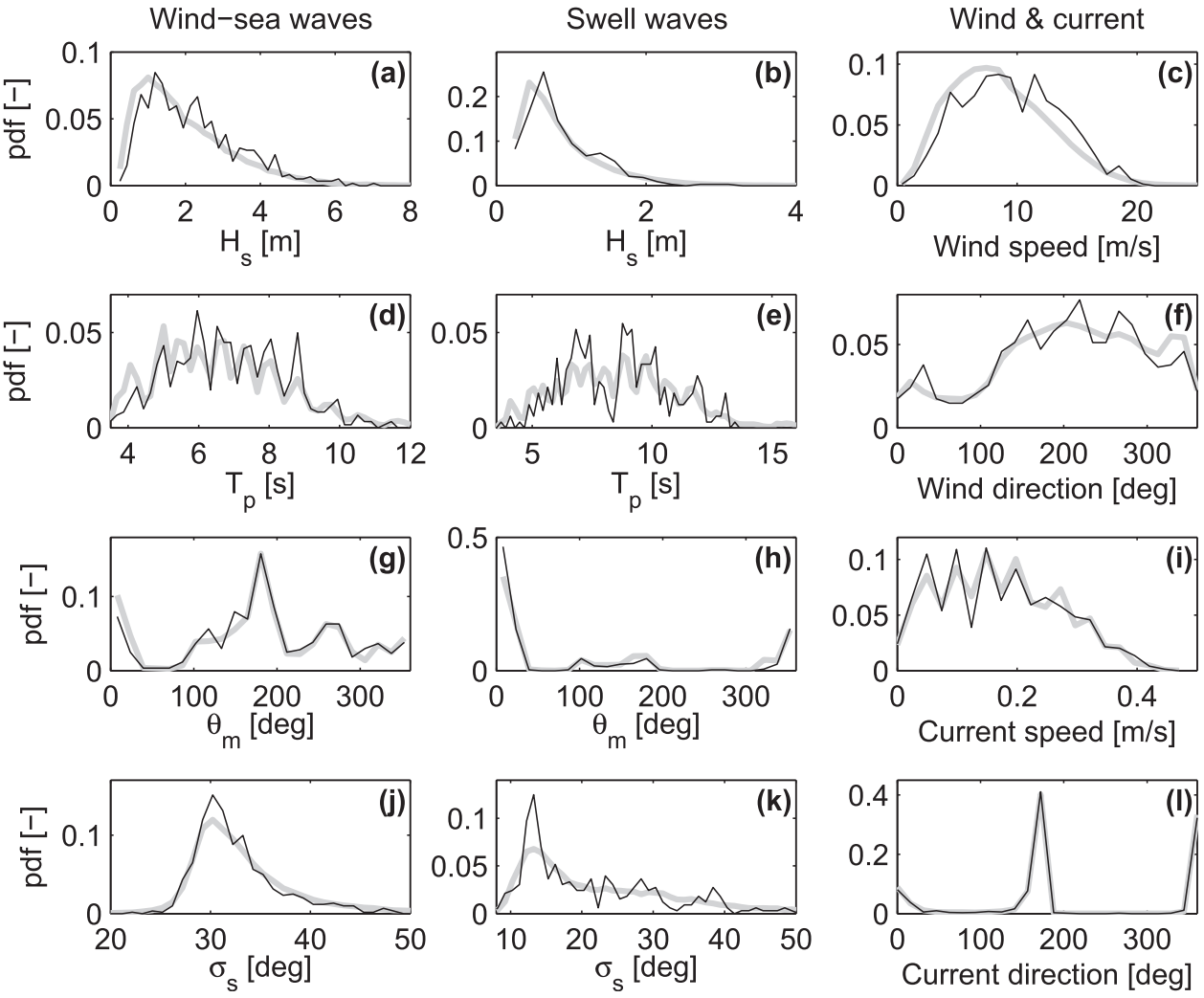

FIG. 4. Empirical probability density functions of the absolute environmental conditions for normal wave samples (gray line) and rogue wave samples (black line). The significant wave height H_s, peak period T_p, mean direction of propagation θ_m, and directional spreading σ_s for the wind-sea components are presented in the first column and for the swell partition in the second column. The third column illustrates the wind speed and direction as well as the current speed and direction.

c. *Local parameters*

It has been demonstrated that there is no convincing evidence to suggest a link between the sea state conditions and the likelihood of a rogue wave event. Consequently, the local parameters in the vicinity of the rogue wave will now be examined to ascertain whether these have a strong influence. Consider first the individual wave steepness, which is illustrated in Fig. 1b. This figure plots the individual wave height against the wave period for all waves that passed the QC checks and distinguishes between the normal and rogue waves. The commonly applied, limiting, one-seventh curve is also shown simply as an indication of the individual wave steepness, though strictly this limit is only applicable for deep-water regular waves. A more rigorous approach for all water depths takes the form of a Miche–Stokes-type limit, as described in Tayfun (2008) and Cherneva et al. (2009, 2013), who have demonstrated that field and experimental measurements of large waves do not exceed this limit. In contrast to the sea state steepness, Fig. 1b demonstrates that the rogue waves are typically steep with some very close to the one-seventh steepness. However, while the rogue waves are steep, there is still a large quantity of normal waves that are at least as steep that do not become rogues. Therefore, local steepness alone, and consequently increased nonlinearity, does not appear to explain the formation of rogue waves.

Another local aspect of interest is the average shape of rogue waves and how it differs from the largest normal

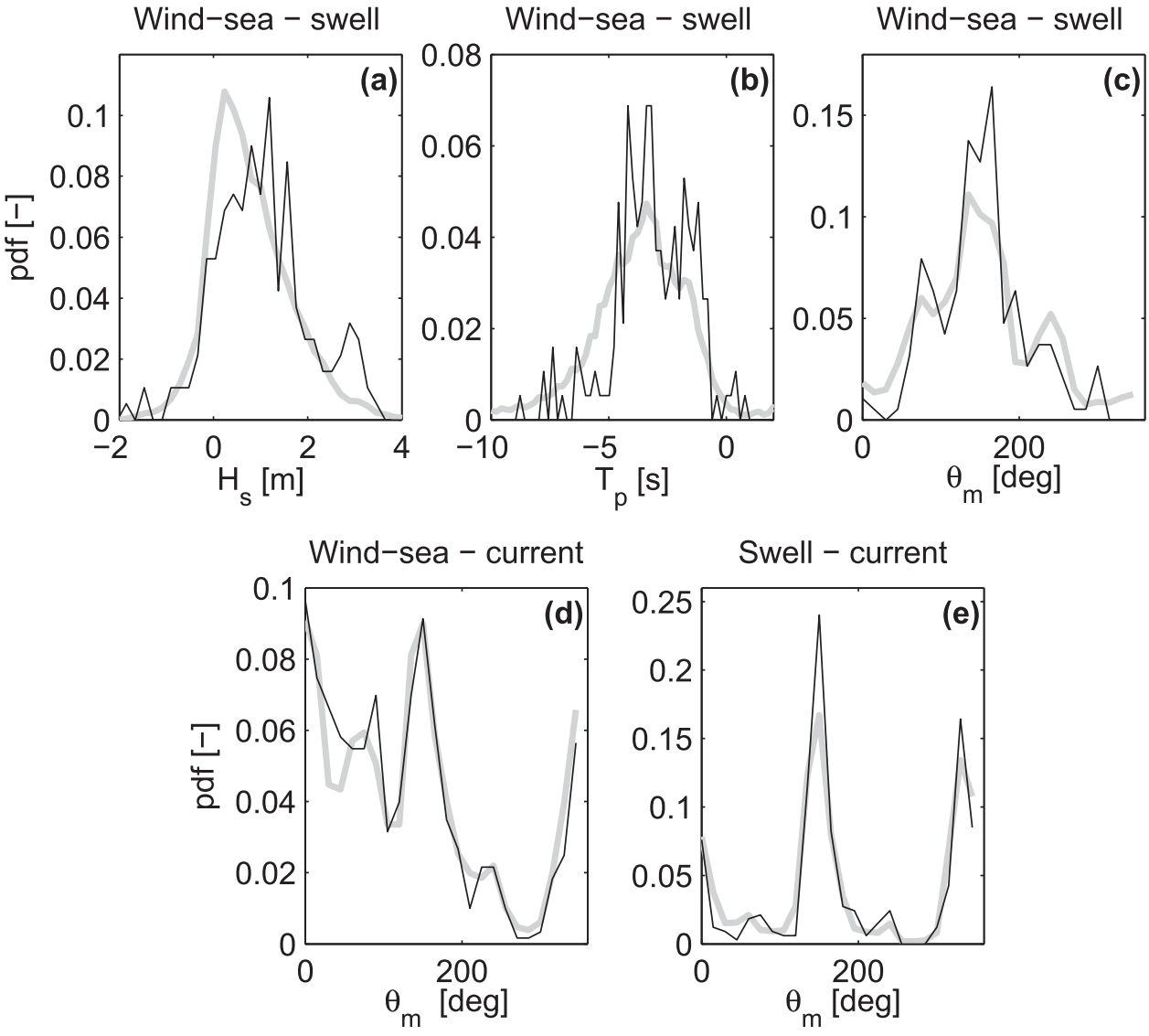

FIG. 5. Empirical probability density functions of the relative environmental conditions for normal wave samples (gray line) and rogue wave samples (black line). (a) Significant wave height H_s from wind sea minus swell partitions; (b) peak period T_p from wind sea minus swell partitions; (c) mean direction of propagation θ_m from wind sea minus swell partitions; (d) mean direction from wind sea minus current; and (e) mean direction from swell minus current.

waves. It has long been known that the average shape of the largest waves in the ocean is the scaled autocorrelation function (Lindgren 1970; Boccotti 1983, 2000), which takes the form of a focused crest event and is also referred to as a *new wave* event (Tromans et al. 1991). This has already been validated against field measurements for normal wave samples (Jonathan et al. 1994; Jonathan and Taylor 1997).

Figure 6 presents the average shape of the rogue wave crests compared to the largest 1% of normal waves within the present database (corresponding to 5286 samples); the surface elevation being normalized by H_s and time by T_p. This figure has several interesting features. First, it illustrates that the average rogue wave shape also takes a new wave form in the same manner as the largest normal waves. This provides yet another aspect in which normal and rogue wave events do not differ. Second, the average rogue wave shape has higher crests and deeper troughs than the largest normal waves. This implies that the difference cannot be attributed to effects described by Walker et al. (2004), who developed a nonlinear new wave surface profile, as this creates larger crests but shallower troughs, which is not consistent with Fig. 6. This is not meant to suggest that

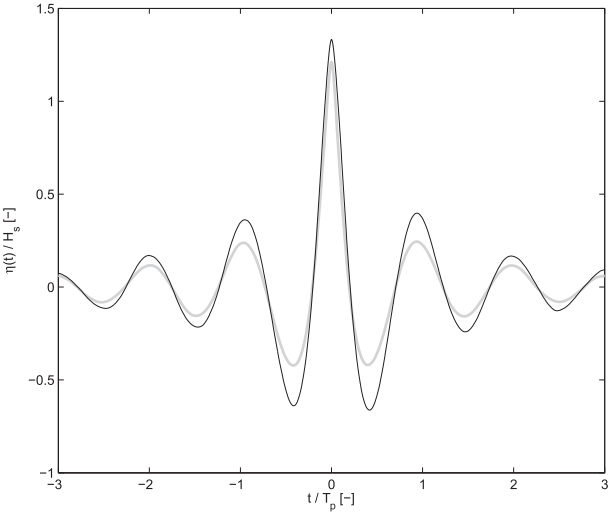

FIG. 6. Average wave shape of the highest 1% of crests in normal sea states (gray line) and from all rogue crests (black line).

nonlinear effects are not present, only that the difference between the average rogue waves and largest normal waves cannot be attributed to nonlinear effects. Third, the normalized wave periods of the average rogue event in Fig. 6 are almost identical to those for the highest normal waves. This indicates that the average rogue wave event is locally steeper than the largest normal waves, which agrees with Fig. 1b and the previous discussion. However, as noted above, the difference in shape of the average rogue wave event is not consistent with nonlinear transformations. This could be explained by a difference in the spectral bandwidth, with the rogue wave samples being more narrowbanded than the highest 1% of normal waves. This can be determined by assessing the spectral width parameter in terms of ε or ν as defined by Cartwright and Longuet-Higgins (1956) and given by

$$\varepsilon = \sqrt{\frac{1 - m_2^2}{m_0 m_4}}, \quad \text{and} \tag{3}$$

$$\nu = \sqrt{\frac{m_2 m_0}{m_1 (m_1 - 1)}}, \tag{4}$$

where m_0, m_1, m_2, and m_4 are the zeroth-, first-, second-, and fourth-order spectral moments, respectively. Figure 7 presents the empirical probability density functions of ε and ν for the highest 1% of normal waves and the rogue wave samples. It can be seen that the two distributions for ε are very similar. As this parameter is related to the local maximum and minima of the water surface elevation, it appears that there is little difference between the largest normal waves and rogue waves in this respect. This is not surprising given that extreme waves tend to be more narrowbanded and thus more regular (Tayfun 2008). In contrast, the rogue waves demonstrate lower values of the ν parameter, indicating that they are more narrowbanded. This provides evidence to suggest that the spectral bandwidth does play a role in distinguishing rogues waves from the largest normal waves.

An additional explanation could be that during the formation of a rogue wave, a larger proportion of frequency components are in phase. This could also include the high frequencies, which will have a negligible effect on periods within the wave group, but they can lead to considerable increases in amplitude if they are in phase with the other frequency components. To examine this in more detail, the local spectrum and phase information in the vicinity of the rogue wave events was analyzed using a time–frequency signal processing technique. In the present study, the wavelet transform was selected along with the complex Morlet wavelet (Liu 2000; Krogstad et al. 2006; Christou et al. 2008). Before applying the wavelet transform, it is first informative to present water surface elevations for three rogue waves events that are representative of the broad range of rogue wave samples from within the database. On its left axes, Fig. 8 presents the water surface elevation $[\eta(t) = a(t)\cos\varphi(t)]$, its Hilbert transform $[\hat{\eta}(t) = a(t)\sin\varphi(t)]$, and the upper and lower wave envelopes all normalized with respect to the root-mean-square of the water surface η_{rms}. In addition, on its right axes, Fig. 8 illustrates the time-varying phase $\varphi(t)$. In this figure, the maximum crest occurs at $t_{\max}$, and the abscissa is normalized with respect to the peak period of each of the sea states in which the rogue waves formed. All three rogue waves demonstrate a maximum crest coinciding with the maximum wave envelope and corresponding to a value of $\hat{\eta} = 0$ and $\varphi = 0$. This is in keeping with the findings of Tayfun (2008) based on second-order theoretical models.

Figure 9 illustrates the results of applying the wavelet transform to the same three example rogue wave events as presented in Fig. 8. In each subfigure, the local spectrum is shown along with the phase of all frequency components at a given instant in time; the ordinates of the former are displayed on the left y axis and of the latter on the right y axis. Figures 9a–c illustrate the local spectrum and phase one peak period before the rogue wave event; Figs. 9d–f are at the time of the rogue wave event; and Figs. 9g–i are for one peak period after the rogue wave event.

It can be observed from Figs. 9d–f that at the time of the rogue wave event almost all frequency components with nonzero spectral values are approximately in phase with one another; this is also true for the high frequencies

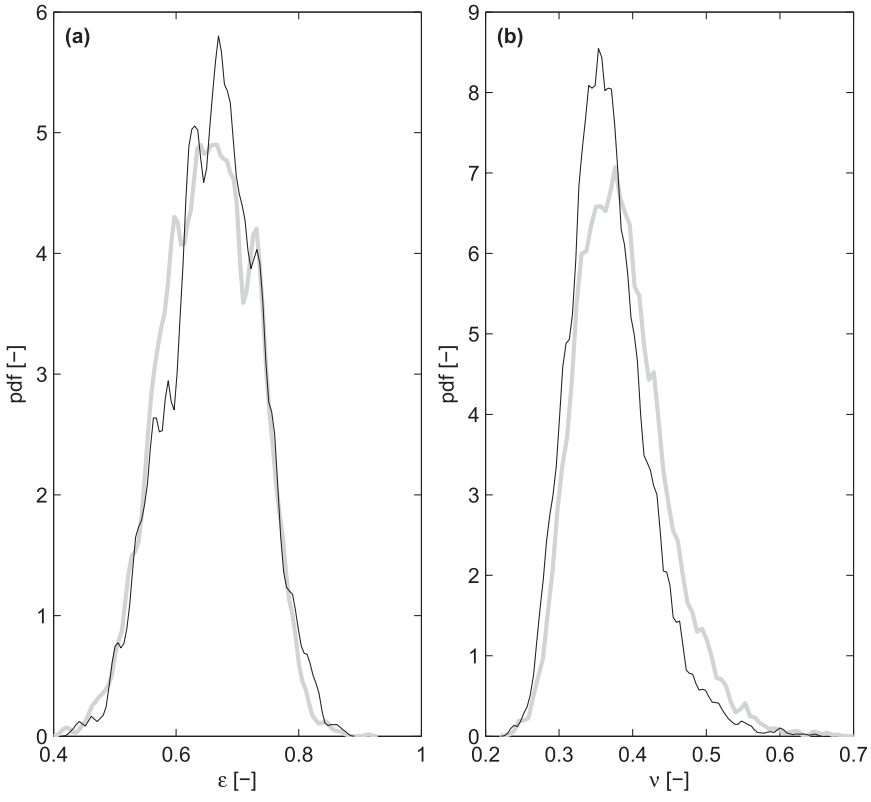

FIG. 7. Empirical probability density function of the spectral width in terms of (a) ε as defined in Eq. (3) and (b) ν given by Eq. (4) of largest 1% of normal waves (gray line) and rogue waves (black line).

and confirms the discussion above concerning the average shape of rogue waves. Figure 9d is an example of a focused crest event, with the phases around 0°. Figure 9e has phases at approximately 30° and Fig. 9f has phases around 60°. These three figures illustrate that at the time of the rogue wave event there is focusing of the energetic frequency components. They may not always correspond to a phase of zero, but the energetic frequency components are in phase with each other. These three figures present the range of phases about which focusing occurred within the database. Considering Figs. 9a–c as well as Figs. 9g–i for the phases one peak wave period either side of the rogue wave event, there is a positive gradient before and a negative slope of the phase after all of these focused events. This is a very familiar pattern that occurs due to linear dispersion.

To quantify the degree to which frequency components are in phase with each other at the time of a maximum event, the standard deviation of the phases at that instant may be calculated. This corresponds to the phases within Figs. 9d–f for the three example rogue waves considered above. This calculation was performed for all rogue events and the highest 1% of normal waves and will be referred to as σ_{phase} hereinafter. A low value of σ_{phase} indicates that the frequency components are in phase with each other and represents a focused wave, whereas a high number suggests a large variation of the phases and a nonfocused event. The value of σ_{phase} is a function of the number of frequency components included in its calculation. If only the peak frequency is taken this value would equal zero, whereas if all frequency components resulting from the wavelet transform were included, then σ_{phase} would be very large, as this would include frequencies with very low variance density, whose phases are erratic.

Therefore, σ_{phase} will be calculated for an increasing number of frequency components. The number of frequency components n_{phase} is determined by considering only those with a variance density within a given percentage of the spectral peak value; this percentage will be denoted as the variable α hereafter. When α has a low value, this represents only the frequency components very close to the spectral peak. In contrast, a high value of α includes most of the variance–density spectrum. For example, $\alpha = 10\%$ represents the frequency components with variance density greater than or equal to $0.9S_p$, where S_p is the peak spectral value. Similarly, $\alpha = 95\%$ considers all frequencies with variance density greater than or equal to $0.05S_p$.

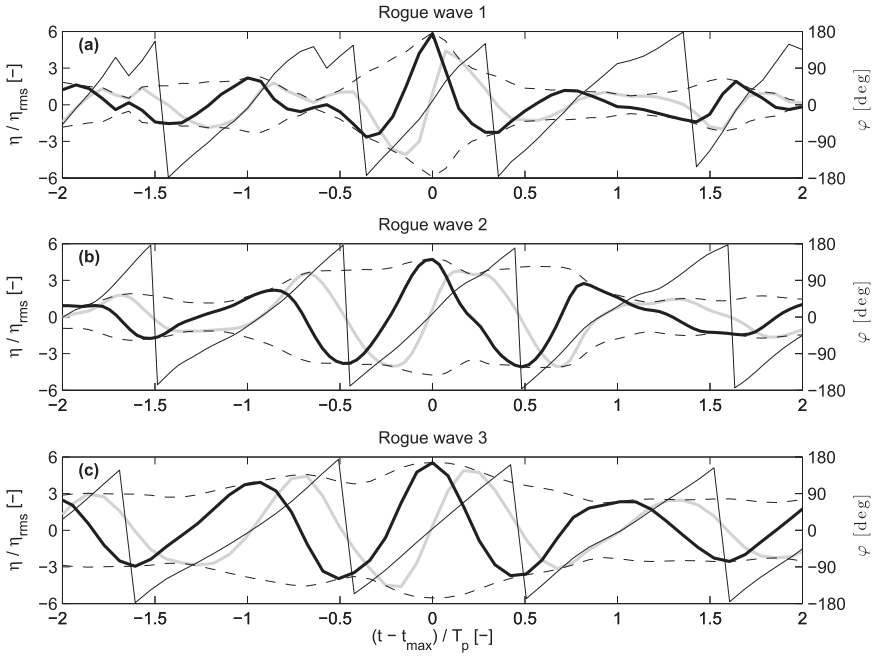

FIG. 8. Three rogue wave examples illustrating on the left axis surface elevation, $\eta(t)$ (thick black line), Hilbert transform $\hat{\eta}(t)$ (thick gray line), and the upper and lower wave envelope (dashed black lines) and on the right axis phase $\varphi(t)$ (thin black line). All of the elevations are scaled with respect to the root-mean-square of the water surface elevation η_{rms}. The largest rogue wave event occurs at t_{max}, and the time axis is normalized with respect to the peak period T_p.

Figure 10 presents empirical probability distributions of σ_{phase} for the highest 1% of normal waves and the rogue events as a function of α. It can be observed that for low values of α in Figs. 10a–c both probability distributions are very similar. In contrast, as α increases to larger values, as in Figs. 10g–i, the probability distributions differ with a higher number of rogue wave events having lower values of σ_{phase}. This is summarized in Fig. 11a, which presents the mean of σ_{phase} as a function of α for the highest normal waves and rogue events. This figure clearly demonstrates that as α increases, the difference between the normal waves and rogue events increases, with the rogue waves having lower mean values of σ_{phase}. This suggests that rogue waves are generated when a larger number of frequency components are in phase with each other.

This difference in standard deviation could be due to the number of frequency components n_{phase} in the calculation of σ_{phase}. This is illustrated in Fig. 11b, and it can be observed that for α less than 60%, this value is identical for both the highest normal waves and the rogue waves. Consequently, this cannot be responsible for the difference in mean σ_{phase} that is observed in Fig. 11a, but it indicates that the components are more in phase at the time of a maximum event than for the highest 1% of normal waves. Note that the difference in the mean value of σ_{phase} between the normal and rogue events is not that large. However, it is sufficiently large to cause the rogue wave events to exceed the threshold defined by the rogue wave criteria. This further indicates that rogue waves are simply rare occurrences of the normal wave population.

Therefore, evidence from the present study has demonstrated that rogue wave events are not governed on a sea state level, but are caused by local effects and in particular by dispersive focusing. They are differentiated from the highest normal waves due to increased focusing and a greater number of frequency components being in phase with each other, which is indeed a rare occurrence.

d. Expected number of rogue waves

A crest elevation that looks unlikely when viewed in the context of a 20-min or 1-h interval in which it was found may well be expected in the context of the whole dataset (many intervals of storm history over many locations). The objective of this section is to put the results into a long-term, multilocation context.

Let P be the probability that a random wave sample of N waves contains at least one rogue event:

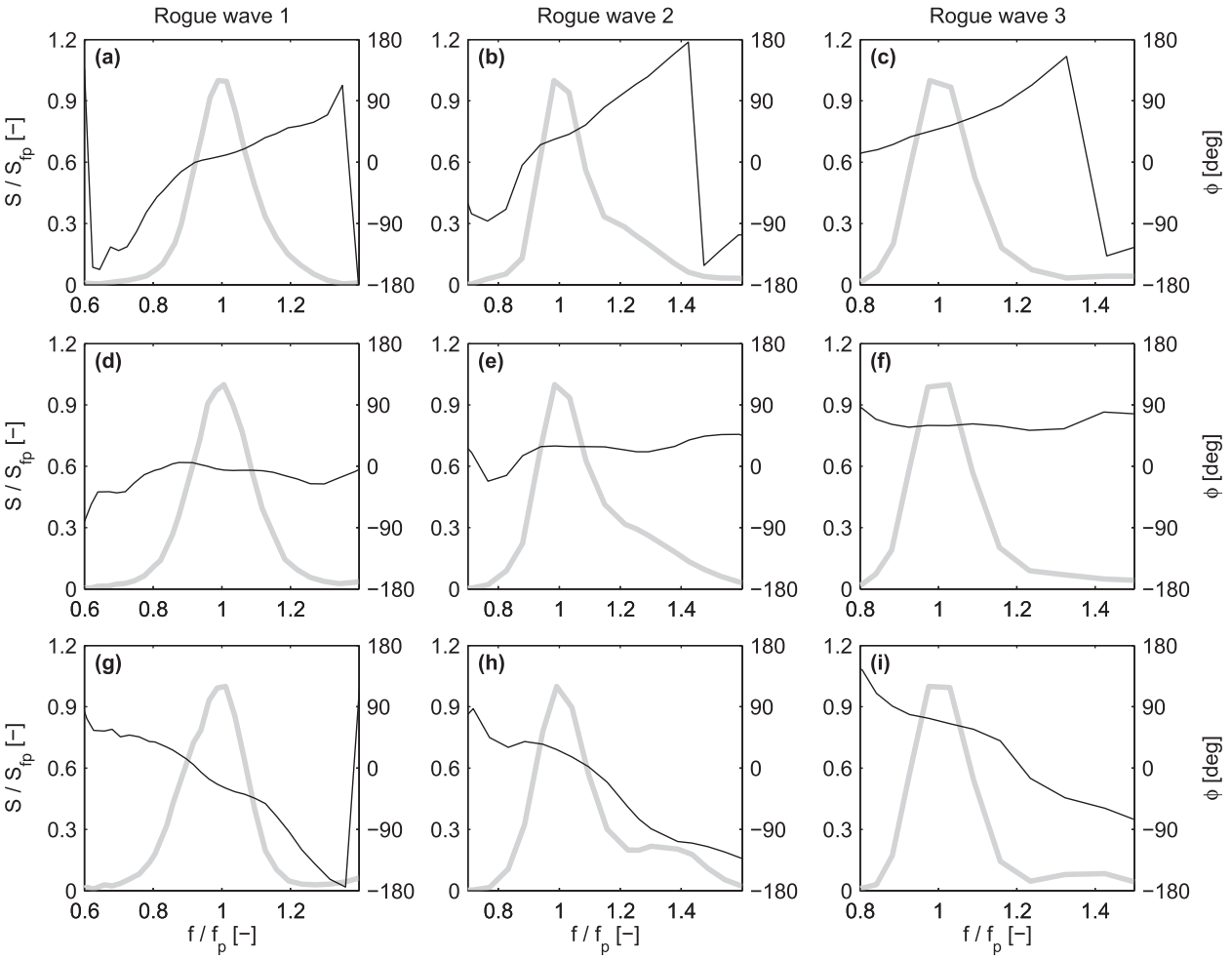

FIG. 9. Wavelet transform results for the variance–density spectra S (gray line) and phases ϕ (black line) of three rogue wave events. The left axis indicates the variance–density spectrum normalized with respect to the peak value, and the right axis represents the phase in degrees. (a)–(c) Occur one wave period before the rogue wave event; (d)–(f) at the time of the rogue wave event; and (g)–(i) for one wave period after the rogue wave event.

$$P = 1 - \left[F\left(\frac{\eta}{H_s}\right)\right]^N, \tag{5}$$

where F is the chosen probability distribution of the normalized crest elevation η/H_s. Now, assuming each record is independent of all other records, the probability b of seeing k records in a total of n is given by the binomial distribution, assuming P is constant for all records:

$$b(k; n, P) = \binom{n}{k} P^k (1 - P)^{n-k}. \tag{6}$$

The most probable number of records can then be taken as the number of rogue wave events we might expect. To perform this calculation, it is necessary to assume a probability distribution for the normalized crest elevation F. For a linear calculation, the Rayleigh distribution can be employed. In this case the probability F of observing $\eta/H_s > 1.25$ is constant, as it only depends on the significant wave height. An improved calculation can be made by using the second-order crest distribution of Forristall (2000). In this case, the probability F is no longer constant, as it will vary because the Forristall distribution depends on the mean steepness and the Ursell number and therefore differs for each sea state. Therefore, the required approach is to calculate the permutations of all values of P for each sea state. For a database with more than half a million sea states, this calculation is prohibitive. Consequently, an efficient approximation is to determine the Forristall distribution for all sea states and then calculate the median distribution. This median Forristall distribution represents F, and the binomial distribution can then be applied in the same manner. For both the linear and second-order approaches, the value of

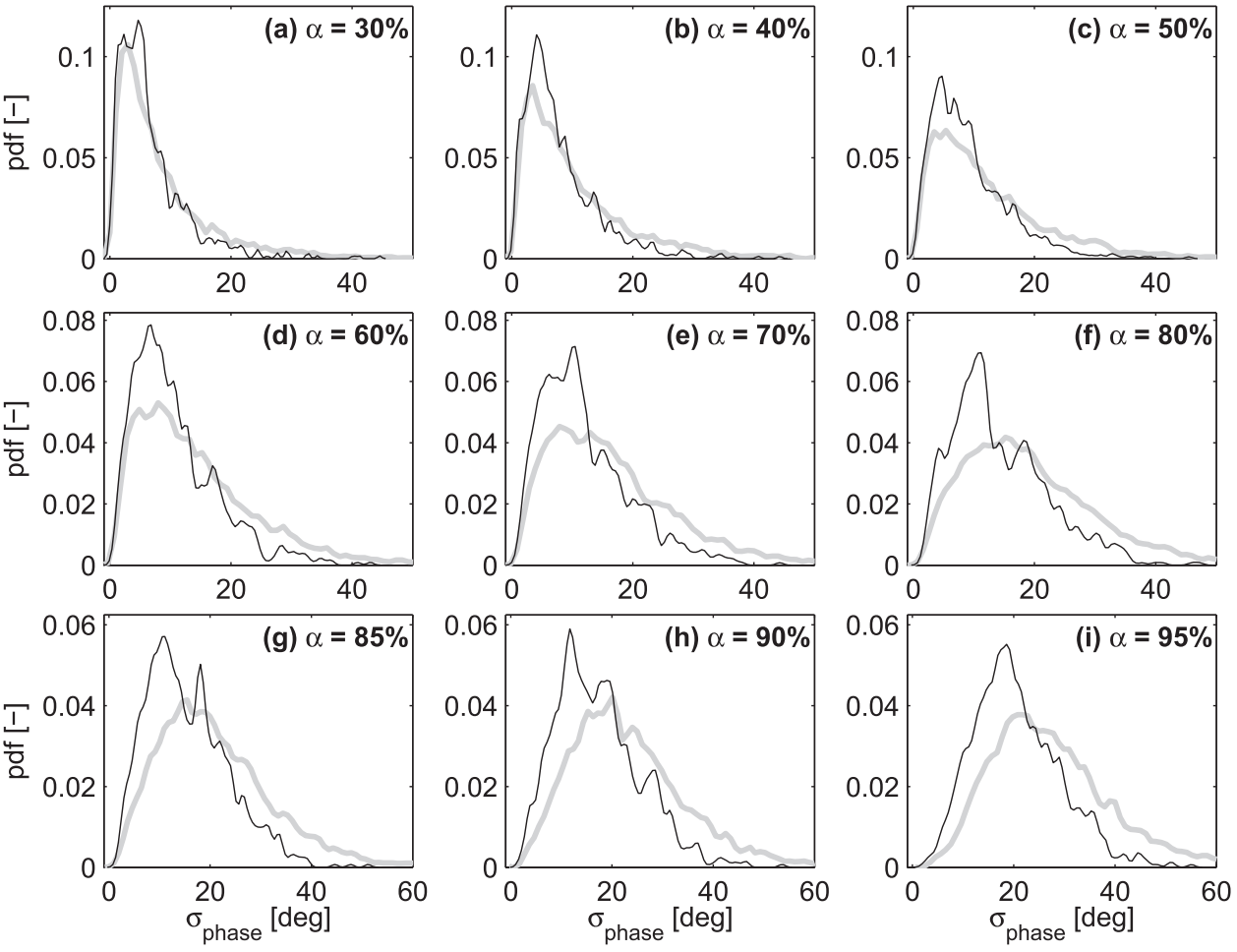

FIG. 10. Empirical probability distributions of the standard deviation of phases at the time of a maximum event σ_{phase} for the highest 1% of normal waves (gray line) and rogue wave events (black line). The various subfigures present the distributions for different values of α.

N is taken as the mean number of waves in a sea state based on the average value across the entire database.

Based on this approach, for the current database the expected number of rogue crests from the Rayleigh distribution is 455 and 1980 for the median Forristall distribution. In contrast, the actual number of observed rogue crests within the database is 745 for $\eta/H_s > 1.25$; note that this does not include the events with only $H/H_s > 2$. Consequently, the measured value lies in between the linear and second-order estimates. Given that the Rayleigh distribution underestimates crest elevation, it is logical that this will also predict a reduced number of rogue waves. The second-order Forristall crest distribution should provide a better estimate; however, it vastly over predicts the number of observed rogue waves. This may be in part due to the approximation of the median Forristall distribution employed to determine the number of rogue events. It may also be due to effects beyond second order such as further nonlinear amplification and wave breaking as demonstrated by Latheef and Swan (2013); the latter effect of breaking leads to crest elevations that lie between the Rayleigh and Forristall distributions. In particular, the result supports the conclusion that the waves are behaving with statistical characteristics somewhat stronger than Gaussian but less than second order. This supports the conclusion of Fedele (2012) and Fedele et al. (2013) that realistic oceanic rogue waves behave statistically as quasi-Gaussian in contrast to the strongly non-Gaussian waves generated in laboratory investigations (Fedele 2008).

5. Conclusions

This paper has described the collation, quality control, and analysis of single-point field measurements from fixed sensors mounted on offshore platforms. In total, the quality-controlled database contains 122 million individual waves, of which 3649 are rogue waves according

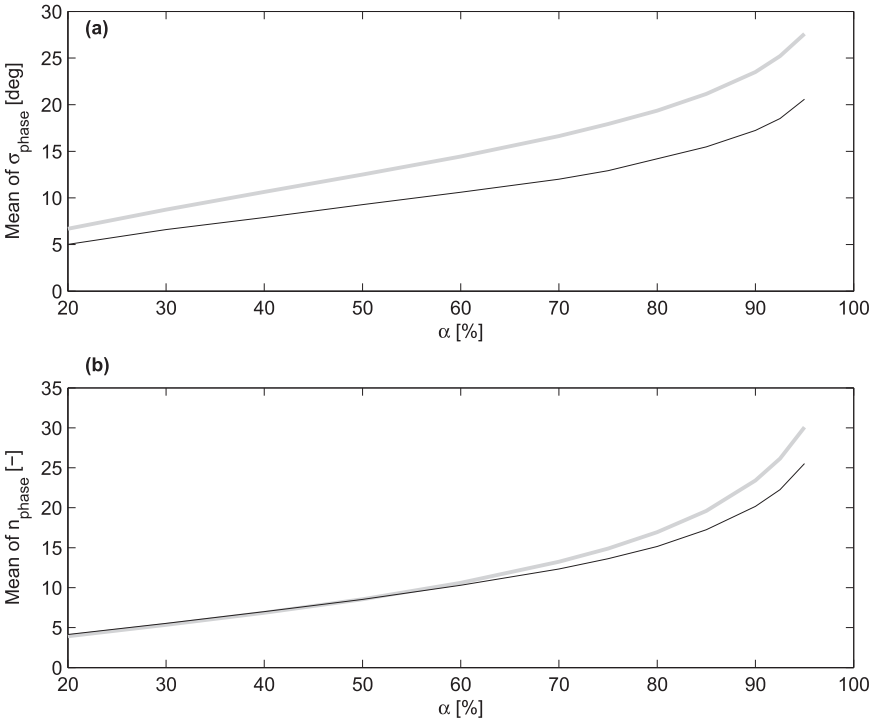

FIG. 11. (a) Mean of the standard deviation of phases at the time of a maximum event σ_{phase} and (b) mean of the number of frequency components n_{phase} employed to calculate σ_{phase} expressed as a function of α for the highest 1% of normal waves (gray line) and rogue wave events (black line).

to the criteria of Haver (2000). A database of this size is necessary in order to ensure a large enough sample of rogue waves, as they are very rare. The majority of the data were measured in the central and southern North Sea, and therefore the results are representative of waves propagating in intermediate water depths within extratropical locations.

To determine physical mechanisms for rogue waves, the sea state parameters were examined. It was found that the occurrence of rogue waves was not a function of the steepness or skewness of the sea state; the kurtosis of the sea state of rogue wave samples had values greater than three. However, the latter is not an indicator for rogue waves, as it is the rogue wave that causes the high kurtosis, which was also demonstrated in the present study following the work of Stansell (2004). The variance–density spectrum for all the rogue waves was also examined, but there was no evidence of a common trend with both uni- and bimodal frequency spectra present. Therefore, neither could be judged to be a mechanism behind rogue waves. On examining the environmental conditions for each sea state, there was no indication to suggest that there was any particular combination of wind sea, swell, wind, or current that is particularly conducive to the formation of rogue waves.

Having determined that the sea state parameters do not play a role in the formation of rogue waves, the local parameters were then examined. It was found that the steepness of the individual rogue waves was greater than the bulk of normal waves. However, there were also normal waves that were as steep as or steeper than rogue waves. Consequently, a rogue wave is generally steeper than normal waves but not all steep waves are rogues. The average shape of rogue waves was also shown to be a new wave profile (Tromans et al. 1991) similar to the largest normal waves and corresponding to a focused crest event. Furthermore, the average rogue wave shape had higher crests as well as deeper troughs than the highest 1% of normal waves. It was also demonstrated that rogue waves were slightly more narrowbanded than the highest 1% of normal waves based on the ν spectral bandwidth parameter.

Finally, a wavelet analysis was performed on all rogue wave samples to ascertain the temporal evolution of the variance–density spectrum and phases. The rogue wave samples exhibit dispersive focusing, resulting in the majority of frequency components coming into phase with each other at the time of the rogue wave events.

In conclusion, the present study has presented evidence to suggest that rogue waves are merely extraordinary and

rare occurrences of the normal population that are caused by dispersive focusing.

Acknowledgments. We acknowledge the participants of the CresT JIP for their continuous support and interesting discussions during the project, without which the present study would not have been possible: ABS Consulting, Aker Solutions, Anadarko, SBM Offshore, BHP Billiton, Bluewater, BP, Bureau Veritas, ConocoPhillips, Det Norske Veritas, Floatec, Forristall Ocean Engineering, HSE, Imperial College London, JOGMEC, Lloyd's Register, MARIN, MMS, Ocean Wave Engineering, Oceanweather, Petrobras, Shell, Sofec, Statoil, Total, Woodside, and WorleyParsonsSea. We are also grateful to the insightful and constructive feedback from the reviewers, who have helped to improve the overall manuscript.

REFERENCES

Adcock, T. A. A., P. H. Taylor, S. Yan, Q. W. Ma, and P. A. E. M. Janssen, 2011: Did the Draupner wave occur in a crossing sea? *Proc. Roy. Soc. London,* **A467,** 3004–3021, doi:10.1098/rspa.2011.0049.

Angevaare, T. J., 1986: The offshore environment: Metocean instrumentation. Shell Tech. Rep.

Boccotti, P., 1983: Some new results on statistical properties of wind waves. *Appl. Ocean Res.,* **5,** 134–140, doi:10.1016/0141-1187(83)90067-6.

——, 2000: *Wave Mechanics for Ocean Engineering.* Elsevier, 496 pp.

Cardone, V. J., and A. T. Cox, 2011: Modeling very extreme sea states (VESS) in real and synthetic design level storms. *Proc. 30th Int. Conf. on Offshore Mechanics and Arctic Engineering,* Vol. 2, Rotterdam, Netherlands, American Society of Mechanical Engineers, 531–544.

Cartwright, D. E., and M. S. Longuet-Higgins, 1956: The statistical distribution of the maxima of a random function. *Proc. Roy. Soc. London,* **A237,** 212–232, doi:10.1098/rspa.1956.0173.

Casas-Prat, M., and L. H. Holthuijsen, 2010: Short-term statistics of waves observed in deep water. *J. Geophys. Res.,* **115,** C09024, doi:10.1029/2009JC005742.

Cherneva, Z., and C. Guedes Soares, 2008: Non-linearity and non-stationarity of the New Year abnormal wave. *Appl. Ocean Res.,* **30,** 215–220, doi:10.1016/j.apor.2008.08.003.

——, M. A. Tayfun, and C. Guedes Soares, 2009: Statistics of nonlinear waves generated in an offshore wave basin. *J. Geophys. Res.,* **114,** C08005, doi:10.1029/2009JC005332.

——, ——, and ——, 2013: Statistics of waves with different steepness simulated in a wave basin. *Ocean Eng.,* **60,** 186–192, doi:10.1016/j.oceaneng.2012.12.031.

Christou, M., K. Ewans, B. Buchner, and C. Swan, 2008: Spectral characteristics of an extreme crest measured in a laboratory basin. *Proc. Rogue Waves,* Brest, France, Ifremer, 165–178. [Available online at http://www.ifremer.fr/web-com/stw2008/rw/Proceedings_Rogue_Waves_2008.pdf.]

——, P. Tromans, L. Vanderschuren, and K. Ewans, 2009: Second-order crest statistics of realistic sea states. *Proc. 11th Int. Workshop on Wave Hindcasting and Forecasting,* Halifax, Canada, U.S. Army Engineer Research and Development Center's Coastal and Hydraulics Laboratory, Environment Canada, WMO/IOC JCOMM, C3:1–11.

Clauss, G., and M. Klein, 2011: The New Year wave in a seakeeping basin: Generation, propagation, kinematics and dynamics. *Ocean Eng.,* **38,** 1624–1639, doi:10.1016/j.oceaneng.2011.07.022.

Crabb, J. A., J. S. Driver, and R. A. Haine, 1983: An intercomparison of six wave recorders at NMI Tower, Christchurch Bay. Institute of Oceanographic Sciences Rep. 154, 74 pp. [Available online at http://eprints.soton.ac.uk/14571/1/14571-01.pdf.]

Donelan, M. A., and A. K. Magnusson, 2005: The role of meteorological focusing in generating rogue wave conditions. *Proc. 14th 'Aha Huliko'a Hawaiian Winter Workshop,* Honolulu, HI, University of Hawai'i at Mānoa, 139–145. [Available online at http://www.soest.hawaii.edu/PubServices/2005pdfs/Donelan.pdf.]

Dysthe, K., H. E. Krogstad, and P. Müller, 2008: Oceanic rogue waves. *Annu. Rev. Fluid Mech.,* **40,** 287–310, doi:10.1146/annurev.fluid.40.111406.102203.

Fedele, F., 2008: Rogue waves in oceanic turbulence. *Physica D,* **237,** 2127–2131, doi:10.1016/j.physd.2008.01.022.

——, 2012: Space–time extremes in short-crested storm seas. *J. Phys. Oceanogr.,* **42,** 1601–1615, doi:10.1175/JPO-D-11-0179.1.

——, A. Benetazzo, G. Gallego, P. Shih, A. Yezzi, F. Barbariol, and F. Ardhuin, 2013: Space–time measurements of oceanic sea states. *Ocean Modell.,* **70,** 103–115, doi:10.1016/j.ocemod.2013.01.001.

Forristall, G. Z., 2000: Wave crest distributions: Observations and second-order theory. *J. Phys. Oceanogr.,* **30,** 1931–1943, doi:10.1175/1520-0485(2000)030<1931:WCDOAS>2.0.CO;2.

——, 2005: Understanding rogue waves: Are new physics really necessary? *Proc. 14th 'Aha Huliko'a Hawaiian Winter Workshop,* Honolulu, HI, University of Hawai'i at Mānoa, 29–35. [Available online at http://www.soest.hawaii.edu/PubServices/2005pdfs/Forristall.pdf.]

Gemmrich, J., and C. Garrett, 2008: Unexpected waves. *J. Phys. Oceanogr.,* **38,** 2330–2336, doi:10.1175/2008JPO3960.1.

Gibbs, R., and P. Taylor, 2005: Formation of walls of water in 'fully' nonlinear simulations. *Appl. Ocean Res.,* **27,** 142–157, doi:10.1016/j.apor.2005.11.009.

Gibson, R. S., and C. Swan, 2007: The evolution of large ocean waves: The role of local and rapid spectral changes. *Proc. Roy. Soc. London,* **A463,** 21–48, doi:10.1098/rspa.2006.1729.

Hanson, J., and O. Phillips, 2001: Automatic analysis of ocean surface directional wave spectra. *J. Atmos. Oceanic Technol.,* **18,** 277–293, doi:10.1175/1520-0426(2001)018<0277:AAOOSD>2.0.CO;2.

Haver, S., 2000: Evidences of the existence of freak waves. *Proc. Rogue Waves,* Brest, France, Ifremer, 129–140.

——, and O. J. Anderson, 2000: Freak waves: Rare realization of a typical population or typical realizations of a rare population? *Proc. 10th Int. Offshore and Polar Engineering Conf.,* Seattle, WA, International Society of Offshore and Polar Engineers, 123–130.

Jonathan, P., and P. H. Taylor, 1997: On irregular, non-linear waves in a spread sea. *J. Offshore Mech. Arct. Eng.,* **119,** 37–41, doi:10.1115/1.2829043.

——, ——, and P. S. Tromans, 1994: Storm waves in the northern North Sea. *Proc. Conf. on the Behaviour of Offshore Structures,* Boston, MA, Massachusetts Institute of Technology, 481–494.

Krogstad, H. E., and S. F. Barstow, 2000: A unified approach to extreme value analysis of ocean waves. *Proc. 10th Int. Offshore Polar Engineering Conf.,* Seattle, WA, International Society of Offshore and Polar Engineers, 103–108.

——, A. K. Magnusson, and M. A. Donelan, 2006: Wavelet and local directional analysis of ocean waves. *Int. J. Offshore Polar Eng.,* **10,** 97–103.

Latheef, M., and C. Swan, 2013: A laboratory study of wave crest statistics and the role of directional spreading. *Proc. Roy. Soc. London,* **469,** 20120696, doi:10.1098/rspa.2012.0696.

Lindgren, G., 1970: Some properties of a normal process near a local maximum. *Ann. Math. Stat.,* **41,** 1870–1883, doi:10.1214/aoms/1177696688.

Liu, P. C., 2000: Is the wind-wave frequency spectrum outdated. *Ocean Eng.,* **27,** 577–588, doi:10.1016/S0029-8018(98)00074-2.

Nikolkina, I., and I. Didenkulova, 2011: Rogue waves in 2006–2010. *Nat. Hazards Earth Syst. Sci.,* **11,** 2913–2924, doi:10.5194/nhess-11-2913-2011.

Olagnon, M., and S. van Iseghem, 2000: Some observed characteristics of sea states with extreme waves. *Proc. 10th Int. Offshore Polar Engineering Conf.,* Seattle, WA, International Society of Offshore and Polar Engineers, 84–90.

Onorato, M., A. R. Osborne, M. Serio, L. Cavaleri, C. Brandini, and C. T. Stansberg, 2006: Extreme waves, modulational instability and second order theory: Wave flume experiments on irregular waves. *Eur. J. Mech. B/Fluids,* **25,** 586–601, doi:10.1016/j.euromechflu.2006.01.002.

Pinho, U. F., P. C. Liu, and C. E. P. Ribeira, 2004: Freak waves at Campos basin, Brazil. *Geofizika,* **21,** 53–66.

Proctor, R., C. Bell, L. Eastwood, J. T. Holt, D. Prandle, and E. F. Young, 2004: UK marine renewable energy atlas: Phase 2—POL contribution. Proudman Oceanographic Laboratory Internal Rep. 163, 26 pp.

Seymour, R. J., and D. Castel, 1998: Systematic underestimation of maximum crest heights in deep water using surface-following buoys. *Proc. 17th Int. Conf. on Offshore Mechanics and Arctic Engineering,* Lisbon, Portugal, ASME, 1–8. [Available online at http://cdip.ucsd.edu/themes/media/docs/publications/journal_articles/Systematic_underestimation_of_maximum_crest_heights.pdf.]

Stansell, P., 2004: Distributions of freak wave heights measured in the North Sea. *Appl. Ocean Res.,* **26,** 35–48, doi:10.1016/j.apor.2004.01.004.

Tayfun, M. A., 2008: Distributions of envelope and phase in wind waves. *J. Phys. Oceanogr.,* **38,** 2784–2800, doi:10.1175/2008JPO4008.1.

Toffolli, A., M. Onorato, and J. Monbaliu, 2006: Wave statistics in unimodal and bimodal seas from a second-order model. *Eur. J. Mech. B/Fluids,* **25,** 649–661, doi:10.1016/j.euromechflu.2006.01.003.

Tomita, H., and T. Kawamura, 2000: Statistical analysis and inference from the in-situ data of the Sea of Japan with relevance to abnormal and/or freak waves. *Proc. 10th Int. Offshore and Polar Engineering Conf.,* Seattle, WA, International Society of Offshore and Polar Engineers, 116–122.

Tromans, P. S., A. Anaturk, and P. Hagemeijer, 1991: A new model for the kinematics of large ocean waves—Application as a design wave. *Proc. First Int. Offshore and Polar Engineering Conf.,* Edinburgh, Scotland, International Society of Offshore and Polar Engineers, 64–71. [Available online at http://www.isope.org/publications/proceedings/ISOPE/ISOPE%201991/I91v3p064.pdf.]

Walker, D. A. G., P. H. Taylor, and R. Eatock-Taylor, 2004: The shape of large surface waves on the open sea and the Draupner New Year wave. *Appl. Ocean Res.,* **26,** 73–83, doi:10.1016/j.apor.2005.02.001.